Biomacromolecules

Article

pubs.acs.org/Biomac

The Effect of Branching (Star Architecture) on Poly(D,L-lactide) (PDLLA) Degradation and Drug Delivery

Jason Burke,[†] Roberto Donno,[†] Richard d'Arcy,[†] Sarah Cartmell,*[,‡] and Nicola Tirelli*[,†]

[†]NorthWest Centre of Advanced Drug Delivery (NoWCADD), Manchester Pharmacy School, University of Manchester, Oxford Road, Manchester, M13 9PT, United Kingdom

[‡]School of Materials, University of Manchester, Grosvenor Street, Manchester, M13 9PL, United Kingdom

Supporting Information

ABSTRACT: This study focuses on the comparative evaluation of star (branched) and linear poly(L,D-lactic acid) (PDLLA) as degradable materials employed in controlled release. The polymers were prepared via ring-opening polymerization initiated by decanol (linear), pentaerythritol (4-armed star) and dipentaerythritol (6-armed star), and processed both in the form of films and nanoparticles. Independent of the length or number of their arms, star polymers degrade slower than linear polymers, possibly through a surface (vs bulk) mechanism. Further, the release of a model drug (atorvastatin) followed zero-order-like kinetics for the branched polymers, and first-order kinetics for linear PDLLA. Using NHOst osteoblastic cells, both linear and star polymers were devoid of any significant toxicity and released atorvastatin in a bioavailable form; cell adhesion was considerably lower on star polymer films, and the slower release from their nanoparticles appeared to be beneficial to avoid atorvastatin overdosing.

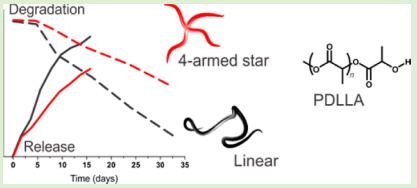

1. INTRODUCTION

This study focuses on the influence of polymer topology on functional properties, and more precisely on whether a single-point branching (star architecture) can affect the performance of a noncrystallizable and degradable polyester structure (poly(D,L-lactic acid), PDLLA) as a matrix for drug delivery.

Branching can provide a number of advantages, which in the context of polyesters have been recently reviewed by us.[1] In short, they include: (a) a higher degree of functionality, which is advantageous for the conjugation/complexation of therapeutically active compounds and the appropriate presentation of groups capable of biological targeting or evasion (e.g., from the mononuclear phagocytic system (MPS)); (b) enhanced stability of micellar self-assembly, in principle allowing for the preparation of unimolecular micelles;[2,3] (c) reduced viscosity at high concentration.

Although significant efforts have been made in the synthesis and physicochemical characterization of branched and, above all, star aliphatic polyesters (as reviewed by Cameron in 2011[4]), to date comparatively little attention has been paid to whether the mechanism of hydrolytic degradation is affected by the presence of branching points, and whether this may have an influence on the functional properties, e.g., the release of an active principle loaded in the polymer.

The use of polyols (commonly glycerol and erythritol derivatives, but also poly(vinyl alcohol) (PVA)) as initiators in lactone ring-opening polymerization is a common method for synthesis branched/star polymers and has been widely employed;[5−10] nevertheless, the effects of branching on the degradability and drug release of the resulting materials have been considerably less studied, with the group of Kissel being one of the few to extensively investigate the matter in the early 1990s and early 2000s. For example, they showed that branched PLGA produced using glucose or PVA as initiators had a faster *in vivo* degradation than linear analogues,[11] and that star block copolymers of poly(ethylene glycol) (PEG) and poly(glycolic acid-*co*-lactic acid) (PLGA), and PVA−PLGA brushes degraded faster than their linear counterparts.[12] Further, it appears that increasing the length and thus the hydrophobicity of PLGA branches may switch the degradation from a surface to a bulk mechanism.[13] To our knowledge, the glucose-initiated star PLGA is the only member of this family that has reached the stage of commercial exploitation, e.g., in the Sandostatin LAR Depot, a form of microspheres loaded with octreotide (a somatostatin analogue), which received approval for use in the USA by the FDA in 1998 for the treatment of acromegaly and tumor-associated diarrhea.[14]

However, it is often difficult to generalize these findings and point out clear advantages (or disadvantages) of branched structures; for example, the above studies report on constructs that are typically more hydrophilic than most polyesters.

Here we have prepared poly(D,L-lactic acid) (PDLLA) star polymers, comparing their degradation and drug release behavior with that of linear PDLLA derivatives of comparable molecular weight. The star PDLLAs were synthesized from two polyol initiators, i.e., pentaerythritol (tetrafunctional: 4-armed polymers), and dipentaerythritol (hexafunctional: 6-armed polymers), employing 1-decanol for the synthesis of linear polymers used here as a control (Scheme 1). All polymers were processed

Received: October 15, 2016
Revised: December 2, 2016
Published: December 8, 2016

DOI: 10.1021/acs.biomac.6b01524
Biomacromolecules 2017, 18, 728−739

Scheme 1. Branched versus Linear PDLLA Structures Produced via Ring-Opening Polymerization of Racemic Lactide in Toluene, Using Decanol, Pentaerythritol and Dipentaerythritol as Initiators (Top Left)[a]

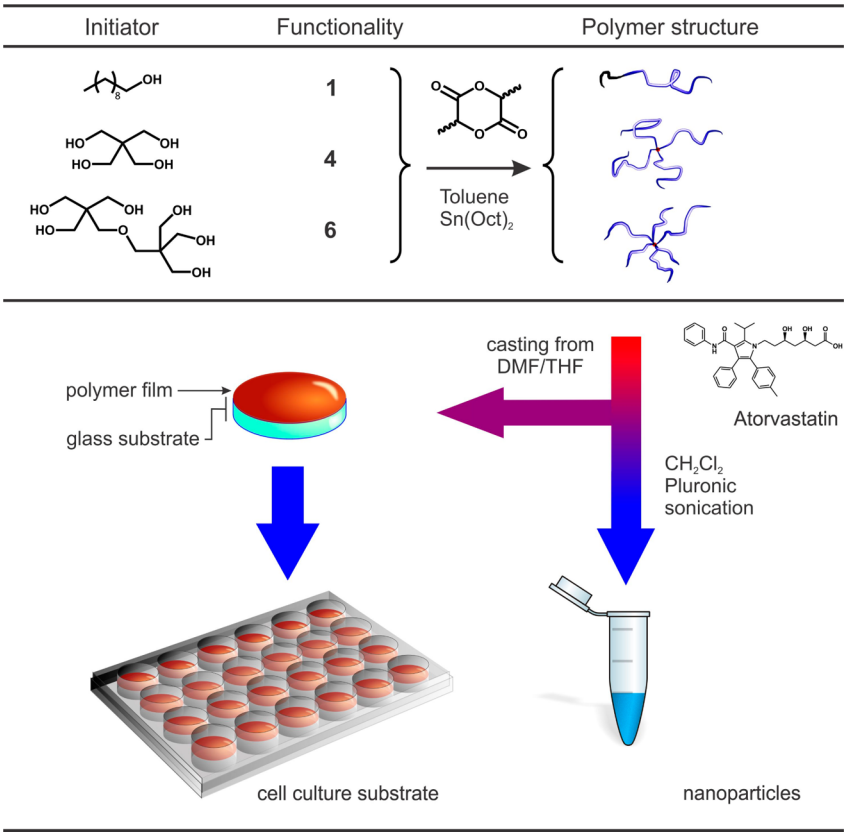

[a]The polymers were then processed in the form of films via solvent casting on circular glass supports for further use in 24-well plates, e.g,. as substrates for cells. After a stage of selection, some polymers were finally produced in the form of nanoparticles through an oil-in-water emulsion method and the use of a PEGylated emulsifier (Pluronic L64).

in the form of homogeneous and transparent films via solution casting.

For drug release behavior, we have selected atorvastatin as a model drug; hydrophobic statins such as atorvastatin and simvastatin are increasingly finding application outside the field of cholesterol control, for example, because of anti-inflammatory activity,[15,16] most intriguingly to stimulate bone formation[17] and therefore also as antiosteoporotic drugs,[18,19] as also demonstrated by previous publications of one of the authors.[20] Although most studies have focused on simvastatin, in this study we have preferred to employ atorvastatin as a model drug, due to its higher (about 2-fold[21]) activity: simvastatin is *per se* inactive and requires the hydrolysis of its lactone ring.

2. EXPERIMENTAL SECTION

2.1. Materials. *Synthesis.* 1-Dodecanol, phosphate buffered solution (PBS), *N*,*N*-dimethylformamide (DMF), *N*-methylpirrolidinone (NMP) (Sigma-Aldrich), hexane, dichloromethane (DCM), and tetrahydrofuran (THF) (Fisher) were used as supplied. Toluene (Fisher) was refluxed under argon over metallic sodium and benzophenone (Fiscer) until the dark purple color of the reduced diphenylketyl radical was stable, and then distilled at 110 °C. Racemic 3,6-dimethyl-1,4-dioxane-2,5-dione (Sigma-Aldrich) was recrystallized twice in dry toluene, dried under vacuum and then stored in a desiccation chamber (phosphorus pentoxide, Fisher) until needed. Pentaerythritol and dipentaerythritol (Sigma-Aldrich) were purified by sublimation under reduced pressure (ca. 10 mbar) at 210 and 220 °C, respectively, and maintained under dry air (desiccator) until needed; tin(II) 2-ethylhexanoate (Sigma-Aldrich) was purified by microdistillation at 140 °C at room pressure and stored under argon.

Cell Culture. NHOst (Clonetics) human osteoblast cells were purchased from Lonza. Fetal bovine serum (FBS), glutamine, antibiotics (Penicillin/Streptomycin), ascorbic acid, β-glycerophosphate disodium salt hydrate (BGP), Dulbecco's modified eagle medium (DMEM), and atorvastatin calcium salt trihydrate were all purchased from Sigma-Aldrich. The Alkaline Phosphatase Activity Assay was purchased from Abcam. The Alamar Blue assay solution was purchased from Life Technologies, while the Bicinchoninic Acid (BCA) kit was purchased from Sigma-Aldrich. Alexa Fluor 488 Phalloidin and Hoechst fluorescent stains were purchased from ThermoFisher for use in microscopy experiments. All other chemicals were purchased from Fisher Scientific.

2.2. Physico-chemical Characterization. *FT-IR.* Spectra were recorded in ATR mode on polymer films obtained by evaporating THF solutions using a heated Golden Gate (120 °C) coupled to a Tensor 27 spectrometer (Bruker).

^{1}H NMR. Spectra were recorded on 10 mg/mL polymer solutions in deuterated chloroform ($CDCl_3$) using a 300 MHz NMR spectrometer (Bruker). Results were analyzed using Mestrenova (Mestrelab) software.

Gel Permeation Chromatography. Gel permeation chromatography was performed on a PL-GPC50 PLUS (Polymer Laboratories) featuring two 0.5 × 30 cm mixed C columns, operated in THF containing 250 ppm BHT, at 30 °C and with a flow rate of 1 mL/min. A universal calibration was carried out using a series of approximately monodisperse linear polystyrene standards. Triple detection (refractive index, viscometer and dual angle light scattering detector at 15° and 90°) was used to obtain absolute molecular weight distributions and Mark–Houwink parameters.

DOI: 10.1021/acs.biomac.6b01524
Biomacromolecules 2017, 18, 728–739

Thermal Analysis. Thermogravimetric analysis (TGA) and differential scanning calorimetry (DSC) were performed on samples produced from polymer films under nitrogen atmosphere at a rate of 5 °C/min, respectively, on a TGA Q500 and on a Q2000 DSC instrument (both TA Instruments). DSC was also used to estimate any crystalline drug possibly present in the polymer matrix.

2.3. PDLLA Synthesis. All polymerization experiments were carried out in a parallel fashion (typically 6 experiments) under mechanical agitation using a Tornado Plus reactor (Radleys). 150 mL vessels were loaded under dry argon with 30 g of 3,6-dimethyl-1,4-dioxane-2,5-dione (0.42 mol) and appropriate amounts of initiators; these corresponded to 16.8 or 8.4 mmol of OH groups for the multifunctional pentaerythritol (4 OH groups), dipentaerythritol (6 OH groups), tripentaerythritol (8 OH groups) and to 4.2 and 2.8 mmol for the monofunctional 1-dodecanol). Twenty-five milliliters of toluene was added always under dry argon, and the vessels were then heated (110 °C in the heating block) under stirring until complete dissolution of the polymer. Five milliliters of a toluene solution of tin(II) 2-ethylhexanoate at appropriate concentration (2-fold molar excess relative to OH groups) was finally added, and the reaction mixture was left stirring at the same temperature for 24 h. After cooling to room temperature, the mixture was diluted with 30 mL of DCM, and the resulting solution was precipitated in cold hexane using 50 mL centrifuge tubes; in each of them, 10 mL of polymer solution were slowly dropped into 20 mL of hexane under stirring. After centrifugation, the process was repeated twice, and finally the samples were placed in a vacuum oven 35 °C, slowly decreasing the pressure to 0.1 mbar and keeping the material under vacuum over a period of 24 Hrs. The powdered samples were kept in a desiccation chamber (P_2O_5) for 24 h, aliquoted, sealed, and stored at 4 °C until needed.

^{1}H NMR ($CDCl_3$): *linear polymers* δ = 0.55−0.65 (*a*, terminal CH_3), 1.15−1.20 (*b*, C**H**$_2$ from dodecane moieties), 1.55−1.65 (*f*, terminal C(H)C**H**$_3$), 1.55−1.75 (*d*, main chain CH(C**H**$_3$), 2.55−2.75 (*h*, CO**H**(terminal)), 4.15−4.25 (*c*, CC**H**$_2$O methylene), 4.30−4.50 (*g*, C**H**(CH_3)terminal), 5.10−5.30 ppm (*e*, C**H**(CH_3)main chain).

4-armed δ = 1.55−1.65 (*f*, terminal C(H)C**H**$_3$), 1.55−1.75 (*d*, main chain CH(C**H**$_3$), 2.55−2.75 (*h*, CO**H**(terminal)), 3.70−3.80 (*c′*, unreacted CC**H**$_2$O methylene) 4.15−4.25 (*c*, CC**H**$_2$O methylene), 4.30−4.50 (*g*, C**H**(CH_3)terminal), 5.10−5.30 ppm (*e*, C**H**(CH_3)main chain).

6-armed δ = 1.55−1.65 (*f*, terminal C(H)C**H**$_3$), 1.55−1.75 (*d*, main chain CH(C**H**$_3$), 2.55−2.75 (*h*, CO**H**(terminal)), 3.35−3.45 (*j*, OC**H**$_2$C dipentaerythritol moiety), 3.70−3.80 (*c′*, unreacted CC**H**$_2$O methylene) 4.15−4.25 (*c*, CC**H**$_2$O methylene), 4.30−4.50 (*g*, C**H**(CH_3)terminal), 5.10−5.30 ppm (*e*, main chain C**H**(CH_3)).

FT-IR (film on ATR crystal): for all polymers 2993 (ν_{as} CH_3), 2943 (ν_{as} CH_3), 2879 (ν CH), 1723 (ν C═O), 1450 (δ_s CH_3), 1385, 1265, 1185 (ν_{as} C−C(═O)−O), 1124 (shoulder, most likely ν_s C−C(═O)−O), 1083 (most likely ν C−C−O) cm^{-1}. For comparison, the monomer bands are located at 3000 (ν_{as} CH_3), 2950 (ν_{as} CH_3), 2895 (ν CH), 1753 (ν C═O), 1445 (δ_s CH_3), 1385 (), 1235 (ν_{as} C−C(═O)−O), 1145 (ν_s C−C(═O)−O), 1092 (ν C−C−O), 1050, 924, 650 cm^{-1}.

2.4. Film Preparation and Characterization. 150 mg of 20% w/v polymer solutions in 90:10 THF/DMF (85:15, 95:5 ratios and NMP in lieu of DMF were also tried, but provided inhomogeneous films) were deposited on ⌀ = 13 mm circular glass coverslips, and the solvent was gradually removed through a stepwise reduction in pressure (from room pressure to 1 mbar in 24 h) in a vacuum oven at 35 °C, and then in a Genevac centrifugal evaporator (10 mbar, 35 °C). Atorvastatin-loaded samples were prepared similarly with the dissolution of drug in the solvent mixture prior to addition to polymer samples. For the release studies, films were prepared to give a loading of 0.1% wt (drug/polymer). The film roughness and thicknesses were assessed using a Dektak-8 (Veeco) profilometer.

Degradation and Drug Release. The films on the circular glass supports were placed in 24-well polystyrene plates and incubated in 2 mL distilled water at 37 °C; please note that at complete release one would have max 15 μg/mL, well below the reported atorvastatin solubility in water (around 1 mg/mL, http://www.drugbank.ca/drugs/DB01076) and therefore under sink conditions). The samples were then removed, dried at room temperature/pressure, weighed, and dissolved in THF to assess polymer degradation via GPC.

0.1% wt atorvastatin-loaded films were used for the release studies. At regular intervals, in each well the supernatant was completely removed and replaced with 2 mL of fresh water; the supernatant was filtered through 0.2 μm PTFE filters and analyzed using an isocratic water/acetonitrile (50:50) mobile phase in a Agilent 1100 HPLC instrument (ChemStation software) equipped with a C18 reverse phase column (Sigma-Aldrich) and a UV/vis detector at 245 nm (Schambeck SFD S3210 UV/vis).

Atomic Force Microscopy (AFM). All measurements were performed at 25 °C with a Molecular Force Probe 3D AFM (MFP-3D Asylum Research, Oxford Instruments, Abingdon, UK). A silicon cantilever, OTESPA (Bruker, Camarillo, CA), with a nominal spring constant of 42.0 N m^{-1} was used both for imaging and for adhesion force measurements. Imaging: all images were acquired in tapping mode in air at a scan frequency of 1 Hz. For each sample, several areas (5 μm x 5 or 3 μm × 3 μm) were imaged. Images were analyzed with Igor-pro/Asylum Research AFM software (Version 13) in order to calculate the root-mean-square (RMS) roughness. Mean and standard deviation values are obtained from at least 3 images. Measurement of adhesion forces: measurements on mica were used to calibrate the deflection sensitivity of the cantilever. The spring constant of the cantilever was calculated with the thermal method and value obtained was equal to 42.8 N m^{-1}. For each sample, several areas were investigated (5 μm × 5 μm or 3 μm × 3 μm) and adhesion force maps were acquired with a spatial resolution of 0.062 μm^2 for the 5 μm^2 images and of 0.022 μm^2 for the 3 μm^2 images (20 × 20 force curves acquired per area). All force curves were acquired with a loading/unloading rate of 1 μm s^{-1}, and the maximum force applied ranged between 50 nN and 70 nN. The adhesion forces between the AFM tip and the surface of the samples were determined from the unloading (retraction) force curves. The difference between the minimum force and the force felt at a large distance from the surface is the adhesion force. Mean and standard deviation values are obtained from at least four different force maps.

2.5. Nanoparticle Preparation and Characterization. In a typical experiment, oil-in-water (O/W) emulsions were prepared my mixing 4 mL of a 10% wt PDLLA solutions in dichloromethane (possibly containing atorvastatin at a target 0.01% wt relative to PDLLA) with 16 mL (4X excess) of 2% wt Pluronic L64 (poly(ethylene glycol)-bl-poly(propylene glycol)-bl-poly(ethylene glycol), $\overline{M_n}$ = 2900 g/mol) aqueous solution under high frequency sonication (23 kHz) in an ice bath. A Soniprep 150 (MSE) probe sonicator fitted with an exponential 3 mm probe tip and working at 15 μA (transformation ratio of 7:1) was used for this purpose; the probe tip was placed approximately 2 cm beneath the surface of mixture. The oil phase (polymer/drug solutions) was added dropwise to the aqueous phase via a buret and the mixture was sonicated for an additional 10 min after the end of the addition. The suspensions were stirred overnight at room temperature (250 rpm) to evaporate dichloromethane, and large aggregates were removed via gentle centrifugation at 125g (RCF) for 5 min; the nanoparticles were then pelleted via centrifugation at 2580g (RCF) for 15 min, washing the pellet with distilled water and repeating the centrifugation twice before filtering the suspension through 0.45 μm filters, centrifuged, aspirated, air-dried, weighed, and resuspended at known concentrations in sterile water. The amount of loaded drug was measured by sampling 1 mL of suspensions, pelleting it in Eppendorf tubes (6048g (RCF) for 10 min), drying the pellet, dissolving it in dichloromethane and finally measuring the atorvastatin absorbance at 245 nm, using nonloaded polymer nanoparticles as blanks and atorvastatin samples as references.

The nanoparticle size was measured using a Zetasizer Nano ZS instrument (Model ZEN2500, Malvern Instruments Ltd.; Malvern, UK) at a scattering angle of 173° and at a temperature of 25 °C. In stability studies, measurements were carried out over a 10 day period in PBS at 37 °C.

Drug Release. A 2 mL aliquot of a freshly prepared 5 mg/mL nanoparticle suspension (1% wt atorvastatin in the nanoparticles) in distilled water was incubated at 37 °C. At different time points, the nanoparticles were pelleted via centrifugation as described above,

DOI: 10.1021/acs.biomac.6b01524
Biomacromolecules 2017, 18, 728−739

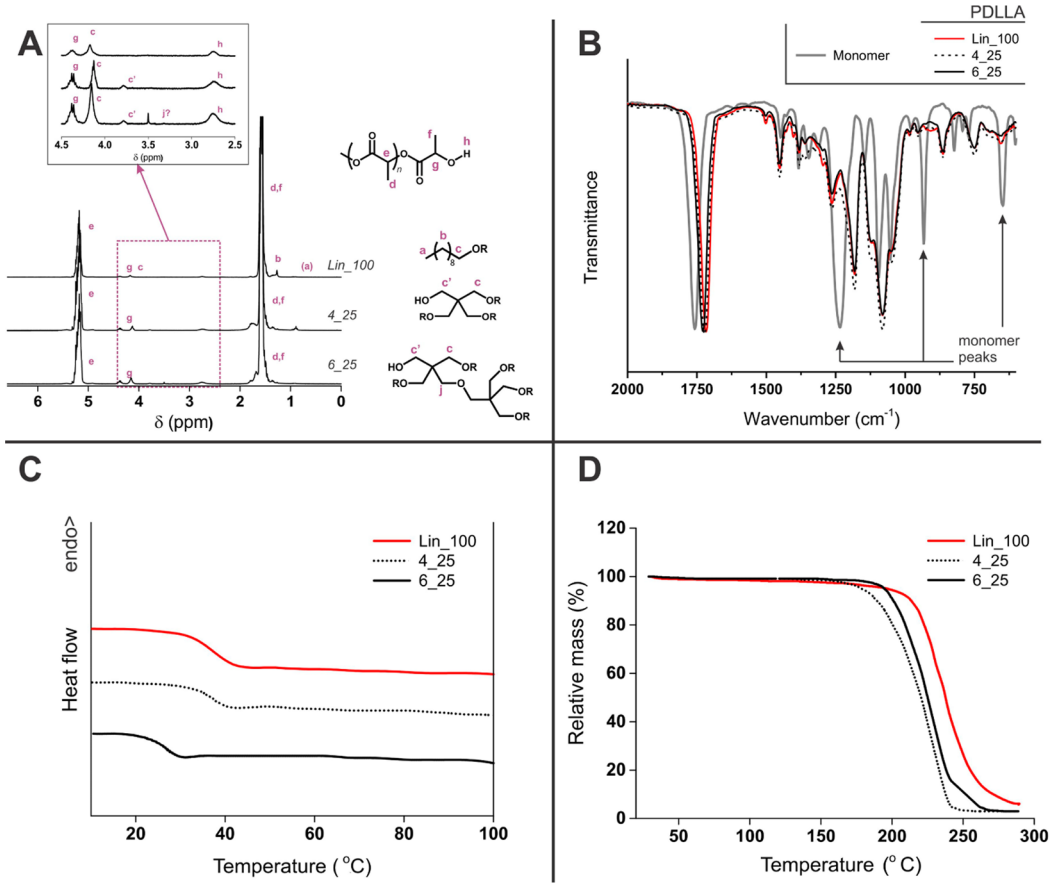

Figure 1. (A) ^{1}H NMR spectra of three PDLLA with different degrees of branching (Lin_100 and 4_25 have similar molecular weight, 4_25 and 6_25 have the same arm length; see Table 1) and assignments of their peaks to the polyester main chain and initiator groups. The inset presents a magnification of the central area of the spectra where end groups resonances can be seen. (B) The different degree of branching in the three PDLLA samples introduced no distinctive feature in the IR spectra, whereas all polymers showed major differences from the monomer spectrum. (C) DSC traces of the three PDLLA samples. All samples contained atorvastatin at a 2.5% wt loading, but no melting peak associated with the drug could be detected in the 120−140 °C region (not shown). (D) TGA traces of the three polymers.

removing the supernatant and replacing it with a fresh 2 mL of aliquot of water. The concentration of the drug in the supernatant was then assessed by measuring the absorbance of the solutions at 245 nm via UV/vis spectroscopy using a PerkinElmer Lambda 35 UV/vis spectrophotometer. Release is presented as a percentage of the average drug content determined previously for any given batch of nanoparticles.

2.6. Cell Culture. *General Procedures.* NHOst cells were cultured in DMEM supplemented with 10% FBS, 1% antibiotics, 2 mM glutamine, 50 μg/mL ascorbic acid and 10 mM BGP. All cells were cultured at 37 °C and under 5% CO_2 and used to maximum passage number of 7.

For experiments performed on supported polymer films, the latter were placed in the wells of 24-well plates, and sterilized by exposing them to decreasing concentrations of ethanol (70, 50, and 20%; 5 min incubation for each concentration). They were then thoroughly rinsed 3 times with PBS prior to the addition of the cells in their culture medium (density = 50 000 cells/well).

For experiments involving polymer nanoparticles, cells were cultured overnight at 60% confluency prior to the addition of treatment. In a typical experiment, 12 5 μL of 1.6, 8, or 16 mg/mL nanoparticle dispersions were added to 125 μL of prefiltered serum-free medium, and the resulting suspension was added to 1.75 mL serum-containing cultures to obtain final nanoparticle concentrations, respectively, of 0.1, 0.5, or 1 mg/mL. The medium was replaced every 3 days with medium containing freshly prepared nanoparticles at the same concentration.

RT-PCR Analysis. PureLink RNA mini kits (Applied Biosystems) were used for RNA isolation, while High Capacity cDNA Reverse Transcription Kits (Applied Biosystems) were used for cDNA synthesis. TaqMan Gene Expression Master Mix was used alongside bone morphogenetic protein-2 (BMP2), runt-related transcription factor-2 (RUNX2), alpha-1-type-1-collagen (COLA1), 18S and Glyceraldehyde-3-Phosphate Dehydrogenase (GAPDH) and TaqMan gene expression assays (Life Technologies) were used for polymerase chain reaction experiments.

Briefly, cells were lysed and RNA was extracted and purified using an RNA extraction kit. Following, RNA was used in reverse transcription to provide cDNA for thermal cycling with TaqMan gene expression assay systems. All reactions were carried out in MicroAmp Fast Optical 96-Well Reaction Plates (Applied Biosciences) and carried out on a StepOnePlus (Life Technologies) RT-PCR analyzer. All reactions were carried out for a total of 40 thermal cycles. Results were run against house-keeping genes (18s or GAPDH) in a ΔΔCT quantitative evaluation method, and all results are expressed as fold change in gene expression relative to negative control samples.

Metabolic Activity. Cells were allowed to adhere to surfaces, cultured for 3 days (on polymer films or exposed to nanoparticle-containing media), analyzed directly using an Alamar Blue reagent following the manufacturers recommendations, and normalized against protein content, which were measured via BCA assay as described above. All results are presented relative to untreated cell samples grown on TCPS.

BCA Assay. Following 8 h incubation after cell seeding, the substrates were washed in PBS to remove unattached cells and any debris, and trypsinized to remove attached cells; the supernatant was centrifuged in 2 mL centrifuge tubes, and the resulting pellets were resuspended in fresh PBS and placed in a 96-well plate alongside the working BCA

DOI: 10.1021/acs.biomac.6b01524
Biomacromolecules 2017, 18, 728−739

Table 1. Physico-chemical Characterization Data for Linear and Branched PDLLA

	no. of arms (NMR)		DP per arm (NMR)		GPC[a]					TGA	DSC
sample[b]	theor	meas[c]	theor[d]	meas[e]	theor. $\overline{M}_n$ (g/mol)[f]	$\overline{M}_n$ (g/mol)	Đ	$[\eta]$ (dL/g)[g]	a[g]	onset (°C)[h]	T_g (°C)[h]
Lin_100	1	=	100	94.8	14,400	15,100	1.17	0.444	1.06	205	42.3
Lin_150	1	=	150	145.0	21,600	22,350	1.27	0.587	0.94	208	44.6
4_25	4	3.60	25	26.9	14,400	15,100	1.06	0.179	0.87	181	39.9
4_50	4	3.52	50	55.3	28,800	29,800	1.11	0.256	0.86	192	41.4
6_25	6	5.26	25	27.9	21,600	23,200	1.11	0.115	0.85	185	30.1
6_50	6	5.02	50	59.1	43,200	47,900	1.14	0.258	0.85	194	34.8

[a]Size distributions can be found in the Supporting Information (Figure S1). [b]Typical conversions: 95% wt for linear polymers, 88−90% wt for 4-armed stars, 84−88% wt for 6-armed stars. [c]Calculated by comparing peak integrals for reacted (c in Figure 1A; δ 4.15−4.25 ppm) and unreacted OH groups (c'; δ 3.8−3.85 ppm). [d]DP (degree of polymerization) per arm calculated as the molar ratio between monomer and alcohol groups in the feed. [e]Calculated by comparing peak integrals for reacted methylene (4.15−4.25 ppm, c in Figure 1A) and main chain methyl groups (1.55−1.75 ppm, d in Figure 1A) and normalizing against the actual no. of arms, as calculated. [f]Calculated as the arm DP * number of arms * molecular weight of the repeating unit. [g]The intrinsic viscosity and the parameter a from the Mark−Houwink equation were obtained via triple detection GPC. [h]Analyses conducted at 5 °C/min. The T_g values are identical in the presence or absence of 1% wt atorvastatin.

solutions. Sample dilutions were carried out where needed. Results were normalized by expressing them as a % of the protein content measured when cells were cultured on TCPS.

Alkaline Phosphatase Assay. An alkaline phosphatase activity assay kit was used to determine the osteoblastogenic activity of NHOst cells in response to the drug-loaded nanoparticles at various concentrations. Measurements were taken after 3 or 7 days of treatment, and enzyme incubation was carried out for 1 h at 25 °C. Results are calculated in terms of enzymatic reaction activity as a function of time.

Fluorescence Microscopy. Cells/films were washed in PBS, and a fixing solution of 4% paraformaldehyde was added to each well for 10 min. Wells were washed thoroughly before being stained with Alexa Fluor 488 Phalloidin (actin) and Hoechst (nucleus) staining solution for 20 min, following manufacturers recommendations. Films were washed in PBS, carefully removed, and placed on glass slides for analysis. Films were coated in PBS throughout the acquisitions to protect cells. Fluorescence microscopy acquisition was carried out on a Leica DMI6000 B inverted microscope equipped with a Leica DFC7000 T 2.8MP color camera and controlled via Micro-Manager software. All images were processed using ImageJ.

3. RESULTS AND DISCUSSION

3.1. Synthesis of Linear and Star PDLLA and Film Preparation. *Polymer Synthesis.* The ROP of polyesters is commonly carried out in the monomer melt at temperatures between 140 and 180 °C, although the use of solvents allows to lower the polymerization temperature to reduce the probability of backbiting and degradation reactions. Pentaerythritol has been successfully employed as a multifunctional initiator for the bulk polymerization of lactides,[22−24] but in pilot experiments we noticed that polyols with higher functionality such as dipentaerythritol and tripentaerythritol (respectively 6 and 8 OH/molecule) were completely insoluble in the monomer. We therefore chose polymerization in a hydrophobic and easy to dry solvent such as toluene, where both pentaerythritol and dipentaerythritol are soluble; tripentaerythritol is only partially soluble and its use as an initiator in refluxing toluene yielded PDLLA with large batch-to-batch variations (although with consistent conversion: 78−82%), thus it was not further employed in this study. Please note that the use of 1-decanol in the preparation of linear polymers was due to the volatility of most monofunctional alcohols, which may result in their poorly reproducible concentration at the polymerization temperature (>100 °C).

Monomer consumption during the polymerization was monitored through FT-IR spectroscopy and showed completion typically <12 h; the final polymers showed the PDLLA characteristic fingerprint region and the complete absence of the lactide ring breathing vibration at 936 cm^{-1} (Figure 1B),[25] ensuring the absence of unreacted monomer in the materials. Six polymers were prepared: two each for linear, 4-armed star, and 6-armed star architecture (Table 1).

The two linear polymers had, respectively, similar molecular weight to the 4-armed and the 6-armed stars with degree of polymerization (DP) = 25. The end group analysis indicated that >80% of the OH groups of the two polyols initiated PDLLA chains, corresponding to an effective degree of branching of around 3.5 for the "4-armed" star polymers and 5 for the "6-armed". For homogeneity, we have nevertheless kept the original nomenclature. The slightly lower degree of branching of the star polymers determined a marginally higher than expected degree of polymerization for each of their arms (compare fourth and fifth column in Table 1). GPC showed that all polymers have monomodal molecular weight distribution (see Supporting Information, Figure S1) with rather narrow dispersity, which would indicate the substantial absence of linear chains initiated by water traces in the reaction environment; the use of triple detection also allowed estimation of the intrinsic viscosity and the Mark−Houwink parameter a, which are both sensitive to the compactness of the polymer coil; as expected (and as previously shown for pentaerythritol-initiated PLLA[26]), the values of both parameters for the star polymers were significantly lower than those for the linear analogues.

Film Preparation. Films were produced from all polymers via solvent casting, with volatiles being evaporated under reduced pressure at 35 °C in a centrifugal evaporator (Genevac EZ-2; SP Scientific) to maximize both efficacy in removal and homogeneity in thickness. Initial attempts with low boiling solvents (THF, DCM, acetone), however, still produced inhomogeneous films, while higher boiling ones (NMP, toluene) often suffered of incomplete removal. At the end of a lengthy optimization procedure, the best results were provided by a 9:1 THF/DMF mixture, which yielded films with a thickness in the range of 350−400 μm with a relative roughness in the range of 0.5−2% (referred to as the film thickness; see Supporting Information, Table S1). Thermal analysis of the six polymers was performed on such films; it highlighted a progressive decrease in glass transition temperature (T_g) with increasing degree of branching (Figure 1C and Table 1), which is probably a result of the lower likelihood of entanglements between the polymer chains; a

DOI: 10.1021/acs.biomac.6b01524
Biomacromolecules 2017, 18, 728−739

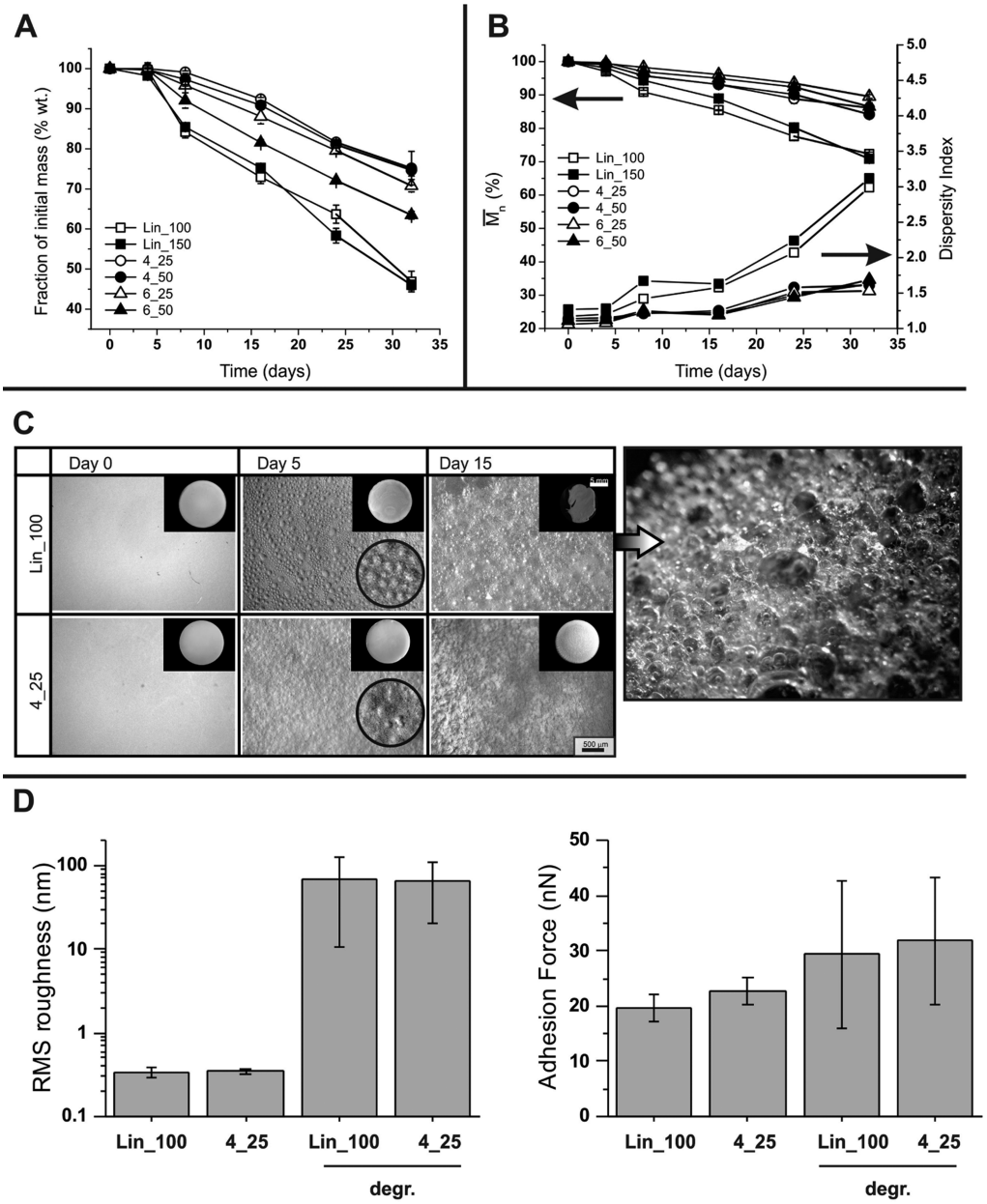

Figure 2. (A) Erosion profile of PDLLA films during hydrolysis at 37 °C. (B). Degradation profiles of PDLLA films at 37 °C. The left axis reports weight-average molecular weight data, the right one those of dispersity index (both from triple detection GPC measurements in THF), and the two arrows link the data points to the respective axes. (C) Low magnification images of Lin_100 and 4_25 film surfaces during the erosion process. At day 7, both PDLLA films developed, and at day 15 the Lin_100 film had lost its overall integrity (small inset) and completely changed its morphology (picture on the right-hand side). On the contrary, the 4-armed star polymer still maintained its shape and developed clear but all-in-all more modest signs of surface degradation; the 6-armed polymers showed an identical behavior (not shown). (D) Roughness (left) and adhesion force to the cantilever (right) as obtained from AFM measurements; the analysis was performed only on two polymers (Lin_100 and 4_25, with virtually identical molecular weight), as representative of the linear and the branched polymers, respectively, since the actual molecular weight of the polymers or the functionality of the branching point seemed to have a negligible role in the degradation behavior. The degraded samples were exposed to water for 7 days.

similar effect has been reported for pentaerythritol-initiated PLLA.[27] A marginal decrease in thermal stability of the branched polymers versus their linear counterparts can also be noted (Figure 1D and Table 1), and may be related to an easier backbiting mechanism of depolymerization in the chain portions near the branching point.

The low temperature of the film preparation process also allows for the incorporation of drugs with minimal risks of thermal degradation. In the films, atorvastatin was typically incorporated at a concentration of 0.1% wt in the polymer; in order to highlight its possible phase separation from PDLLA, we also prepared films with concentrations up to 2.5% wt, which in no case showed any melting endotherm around 135 °C (melting point of the drug), thereby indicating the absence of phase-separated, crystalline drug domains also in the samples with lower drug loadings.

3.2. Degradation of PDLLA Films. Here, we refer to erosion as the loss of solid material, and degradation as the associated reduction in molecular weight. To evaluate the effects

DOI: 10.1021/acs.biomac.6b01524
Biomacromolecules 2017, 18, 728−739

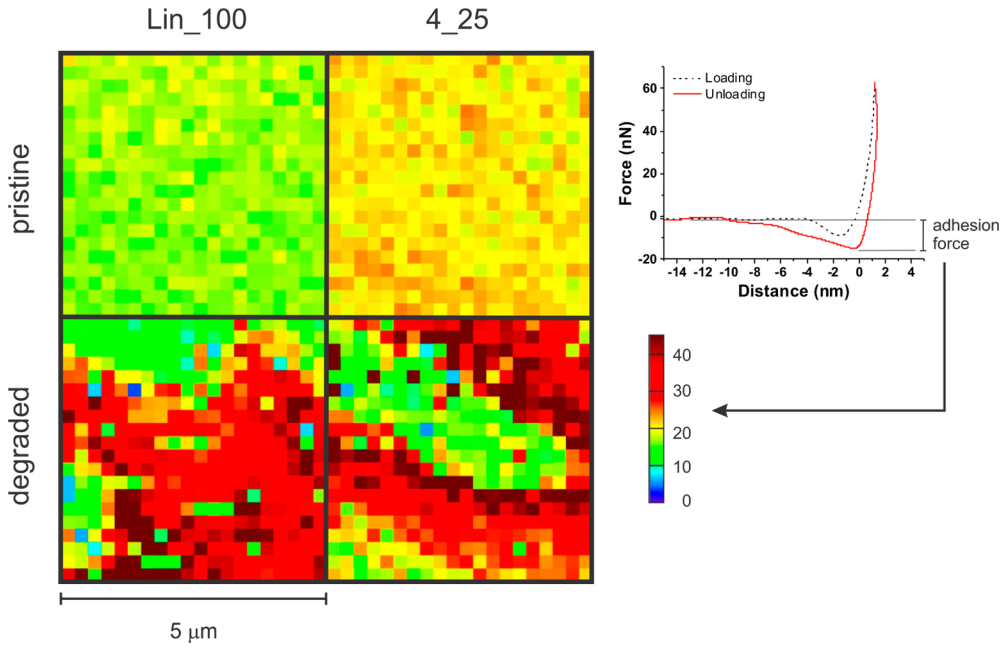

Figure 3. Adhesion maps for Lin_100 and 4_25 PDLLA films following 7 days incubation at 37 °C. The values of adhesion forces were obtained from the differences between loading and unloading nanoindentation curves (a typical example shown in the right part of the figure). The relative elastic modulus maps are presented in the Supporting Information, Figure S2.

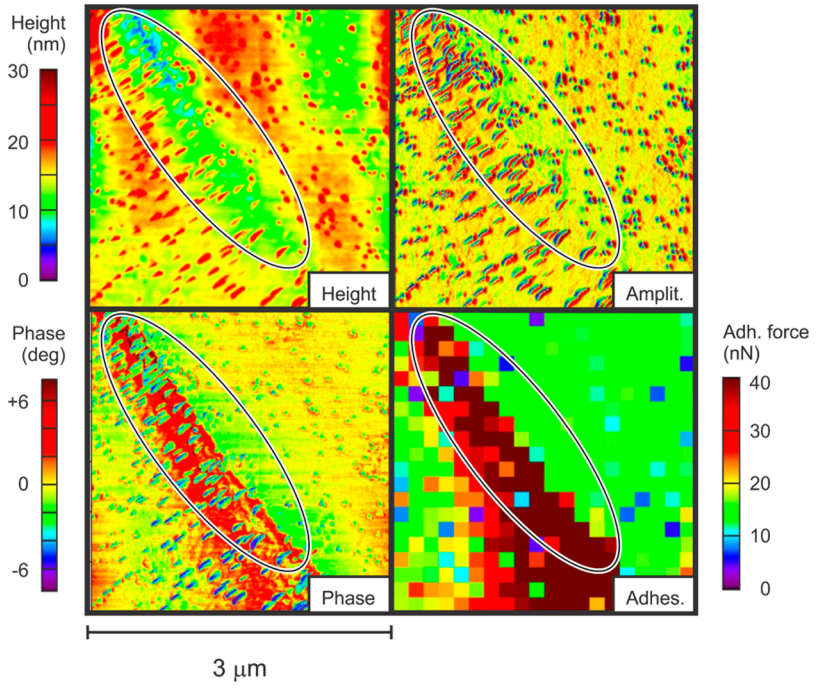

Figure 4. AFM analysis of Lin_100 surfaces during degradation evidenced the presence of domains ranging from a few tens to about 100 nm. These domains are absent in the same polymer before degradation and in 4_25 (either before or during degradation). The panels of the figure report maps of height (top left), amplitude (top right), phase (bottom left) and adhesion force (bottom right) for a 3 × 3 μm area. There, an area of ongoing degradation (oval) can be recognized from its lower height and higher polarity. The domains are present both in this area (possibly in higher number) and in the surrounding regions, and their lower phase values are suggested to be mechanically different from the rest of the polymer. The adhesion force map does not have a sufficiently high resolution to discriminate between these domains and the rest of the polymer, but the presence of a number of isolated low-adhesion points would seem to suggest that the domains are less polar than the surrounding material. The relative elastic modulus maps are presented in the Supporting Information, Figure S3.

of branching on the erosion and degradation of PDLLA, thin films were monitored over time in water at 37 °C.

Both the film erosion (Figure 2A) and the degradation (Figure 2B) of the linear polymers were considerably more rapid than those of their branched counterparts, with at least twice larger reductions in the film mass and in $\overline{M}_n$ at any time point. We ascribe the slower hydrolysis of the star polymers to a decreased solubility of water close to the branching point; by favoring a

DOI: 10.1021/acs.biomac.6b01524
Biomacromolecules 2017, 18, 728−739

nonrandom hydrolysis mechanism (preferred at the chain termini), this would also explain the lower dispersity index of stars in the degradation. Importantly, this is likely to be less noticeable with longer arms.

At a macroscopic level, the accelerated degradation of the linear macromolecules was accompanied by a loss of integrity of their films already by day 15 (small insets in Figure 2C), whereas the branched polymers always retained their shape. Further, the surface of the linear polymer films rapidly covered with cavities and reliefs ("craters" and "bubbles"; see large picture on the right of Figure 2C), which were also visible on branched polymers but in much lower numbers.

AFM was employed for a lower-scale analysis of the surface features of these films (Figure 2D); it is worth pointing out that we were only able to perform this analysis at a relatively early stage of the degradation (up to day 7), because at later time points the high relief of the surface features did not allow reliable AFM measurements. In short, at a submicron scale linear and star polymers provided virtually indistinguishable film morphology and polarity both in the pristine form and during degradation: the surface roughness (Figure 2D, left) showed an identically large increase after 1 week of exposure to water, and also the adhesion force between film surfaces and AFM tip increased for both polymers upon degradation (Figure 2D, right). In the last analysis, large error bars would suggest that the pristine/degraded difference is not statistically significant; at a more careful observation, it is noticeable that the surfaces are very heterogeneous, with very polar areas (red in Figure 3) intermixed with regions similar to the pristine polymers (yellow/green in Figure 3).

The adhesion recorded on the polar areas present only in the degraded samples is more than double that observed in less polar areas or in nondegraded samples, which therefore confirms the heterogeneous (and likely autocatalytic) character of degradation. Further, the polar areas appeared to be softer (lower relative elastic modulus; see Supporting Information, Figures S2 and S3) than the less polar ones and the pristine samples; this is likely a consequence of the presence of traces water plasticizing the material, therefore further confirming that degradation has occurred in these regions.

Only one statistically relevant difference between linear and star polymers was recorded, i.e., the presence of domains with a typical size <100 nm, which appeared only on the surface of the linear polymer films during degradation (Figure 4). We are inclined to consider them as composed of the dodecyl chains present as terminal groups only in the linear polymers: these groups do not undergo hydrolytic degradation, are likely to phase separate from PDLLA, are mechanically different from it and considerably less polar. Nanoindentation would appear to suggest the degraded linear polymers to exhibit lower modulus values (distribution peaked <3 GPa vs around 5 GPa; see Supporting Information, bottom graphs in Figure S2), but the difference is not statistically significant.

For a mechanistic interpretation, it is useful recapitulating that (A) despite their accelerated degradation, mass loss, and loss of integrity, at a submicron level the surface of the linear polymer films seemed relatively similar to that of the star ones, suggesting the presence of similar species, and (B) even when the films of star polymers had lost a significant fraction of their initial mass (e.g., about 30% at day 32), yet the macromolecules exhibited very moderate changes in both the average molecular weight and in its dispersity ($Đ$ always <1.7); nanoindentation can probe materials up the first hundreds of nanometers and may suggest (see Supporting Information, Figure S2) degraded linear polymers to be softer than the branched, whereas the pristine materials are indistinguishable.

Therefore, it appears that the polymer chains remaining in the film were only marginally affected by the hydrolytic process, whereas those on the surface seemed to undergo a degradative process similar to that of linear polymers. It thus appears logical to conclude that the hydrolysis is likely to follow a predominantly surface mechanism in the branched polymers, as opposed to the bulk one normally observed in linear PDLLA. Literature data support this interpretation; for example, Kissel et al. showed that in linear and star PLGA, the water uptake after 36 days of incubation was respectively 21% and 2%.[11] More relevant, Tsuji has recently reached essentially the same conclusion (linear − bulk/branched − surface) utilizing 4-armed star PDLLA produced through bulk polymerization.[28]

3.3. Nanoparticle Preparation. Nanoparticles were produced from oil-in-water emulsions using high-frequency sonication, a well-tested preparative method for polyester nanoparticles.[29] The choice of surfactant can heavily affect not only the colloidal stability but also the drug release kinetics and above all the cellular interactions of the nanoparticles; having, above all, the biological performance in mind, we have selected a PEGylated emulsifier over the more used poly(vinyl alcohol) (PVA); in particular, we have employed Pluronic L64 (PL-64), which presents a hydrophilic−lipophilic balance (HLB) value similar to that of PVA. Tween 20 and Pluronic L-35 were also trialled, but provided broader size distributions. In terms of the surfactant concentration, we have evaluated 1, 2 and 5% wt PL-64, with 1% PL-64 providing significant amounts of precipitates; since 2 and 5% offered indistinguishable results, 2% PL-64 was chosen for all further experiments. The excess emulsifier was removed through a process of multiple pelleting and redispersion (see also Supporting Information, Figure S4), which did not affect the average nanoparticle size or the dispersity of their size distribution.

Since all branched polymers tested had shown a similar degradation behavior, in this part of the study we have only used 4_25 as a polymer matrix, and the Lin_100 as the linear control with identical molecular weight; the two polymers produced nanoparticles with similar size and size distribution (Table 2 and Figure 5A); at the end of the purification process, atorvastatin was still encapsulated with high efficiency in both polymers, and its presence (at 0.01% wt) did not affect the nanoparticle size.

Table 2. Physico-chemical Characterization of Lin_100 and 4_25 PDLLA Nanoparticles

system[a]	recovery %[b]	hydrodynamic size (nm)[c]	polydispersity index (PDI)[c]	encapsulation efficiency/%[d]
Lin_100	90	205 ± 4	0.16	=
Lin_100/AtSt	73	200 ± 5	0.12	76 ± 4.14
4_25	80	175 ± 2	0.13	=
4_25/AtSt	77	175 ± 4	0.12	81 ± 4.04

[a]All samples prepared in the presence of 2% wt Pluronic L64. [b]Reflecting the mass recovery of purified nanoparticles as a fraction of total initial polymer mass. [c]n = 3 different batches. [d]All samples prepared at a target loading of 1% wt.

Finally, we have evaluated the possibility of significant nanoparticle erosion in a time frame relevant for drug release applications; we have therefore followed the size distribution for a period of 12 days (Figure 5B). The occurrence of degradative

DOI: 10.1021/acs.biomac.6b01524
Biomacromolecules 2017, 18, 728−739

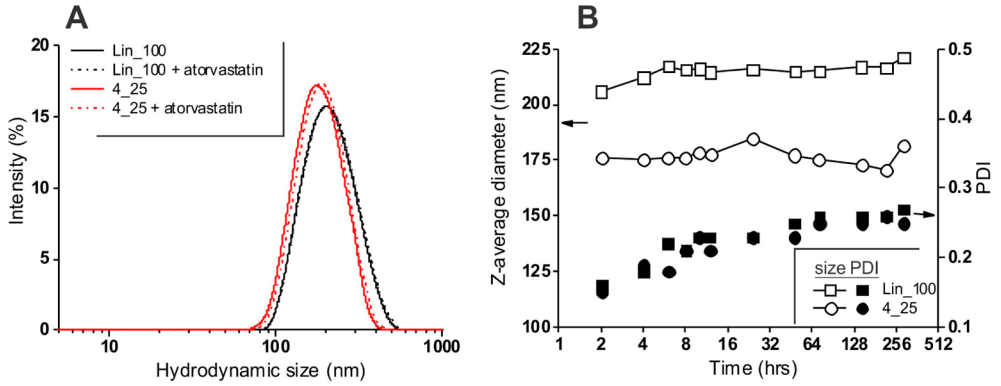

Figure 5. (A) Size distributions for the nanoparticles produced via emulsion method using 4_25 as the branched polymer Lin_100 as its linear analogue. (B) Nanoparticle stability in PBS at 37 °C, as determined by DLS. Black symbols refer to PDI values, white symbols to the Z-average size.

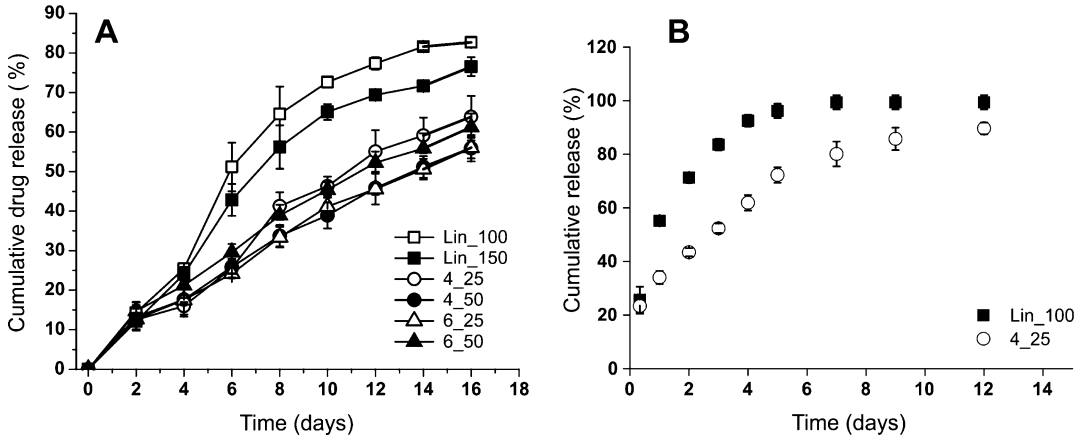

Figure 6. (A) Atorvastatin release at 37 °C in water and under sink conditions from PDLLA films (thickness ≈ 370−380 μm) loaded with 1% wt atorvastatin. (B) at 37 °C in water and under sink conditions from a 5 mg/mL dispersion of PDLLA nanoparticles loaded with 1% wt atorvastatin.

processes can be hypothesized on the basis of the increase in PDI (broader size distribution), although this did not significantly affect the average nanoparticle size. It is noteworthy that, while PDLLA films underwent only a minor degradation at this time point, the vastly larger surface/volume ratio of the nanoparticles is likely to accelerate the hydrolysis kinetics.

3.4. Atorvastatin Release from Films and Nanoparticles. Theoretically, a homogeneously dispersed drug is released from a perfectly surface-degrading matrix through a zero order kinetics (constant release rate). Indeed, the release of atorvastatin from star PDLLA nanoparticles appears to follow such time dependency, whereas first-order kinetics is observed with linear polymers (Figure 5A), which would confirm the difference in the degradation mechanism. The release from polymers, however, is likely to be mechanistically more complex than a simple liberation of drug from the eroded outer layers of the matrix: for example, at day 16, about 50−60% of atorvastatin is released from films, but at that time they would have lost only about 10% of their weight. Therefore, we are inclined to consider the surface degradation of branched PDLLA as one of the factors contributing to the sustained ("zero-order-like") release of the drug, but diffusional factors may also play a significant role. However, diffusional factors are not necessarily related only to the branched PDLLA, as the release of atorvastatin after 16 days from the linear samples was ∼75−80% after only ∼25% degradation with the release of atorvastatin in both linear and branched PDLLA films (Figure 6A) matching the mass loss profile in Figure 2A. This may also be reasoned as an effect of the solvent casting method resulting in a higher density of atorvastatin at the surface of the film.

The release kinetics from both Lin_100 and 4_25 nanoparticles was much accelerated in comparison to those from films (Figure 6B), as would be expected from their much higher surface/volume ratio; additionally, the nanoparticles presented a burst phase, which corresponded to about 20% of the encapsulated drug. However, as seen for the films, branching considerably slowed down the release; the difference was particularly impressive in days 1−4, when the drug released from the Lin_100 nanoparticles was about 70% higher than that liberated from the 4_25 ones. Additionally, at least until day 5, the branched polymer showed zero-order-like release kinetics; this corresponded to at least 50% of atorvastatin being released at a controlled and constant rate.

In short, branching significantly slowed down the release kinetics of atorvastatin from both films and nanoparticles, making it zero-order-like; mechanistically, this is likely to be influenced by the different mechanism of degradation of the star polymers.

3.5. Evaluation of Material Toxicity. We have employed a human osteoblastic cell line popularly used to mimic osteoblastic behavior (NHOst) as the model target of atorvastatin, measuring their day 3 metabolic activity/viability via the Alamar blue assay; the data were normalized against the protein content of the samples, which is related to the cell number and therefore allows providing an activity "per cell". By culturing the cells on PDLLA films, we predominantly assess the effect of (a) cell adhesion/

DOI: 10.1021/acs.biomac.6b01524
Biomacromolecules 2017, 18, 728−739

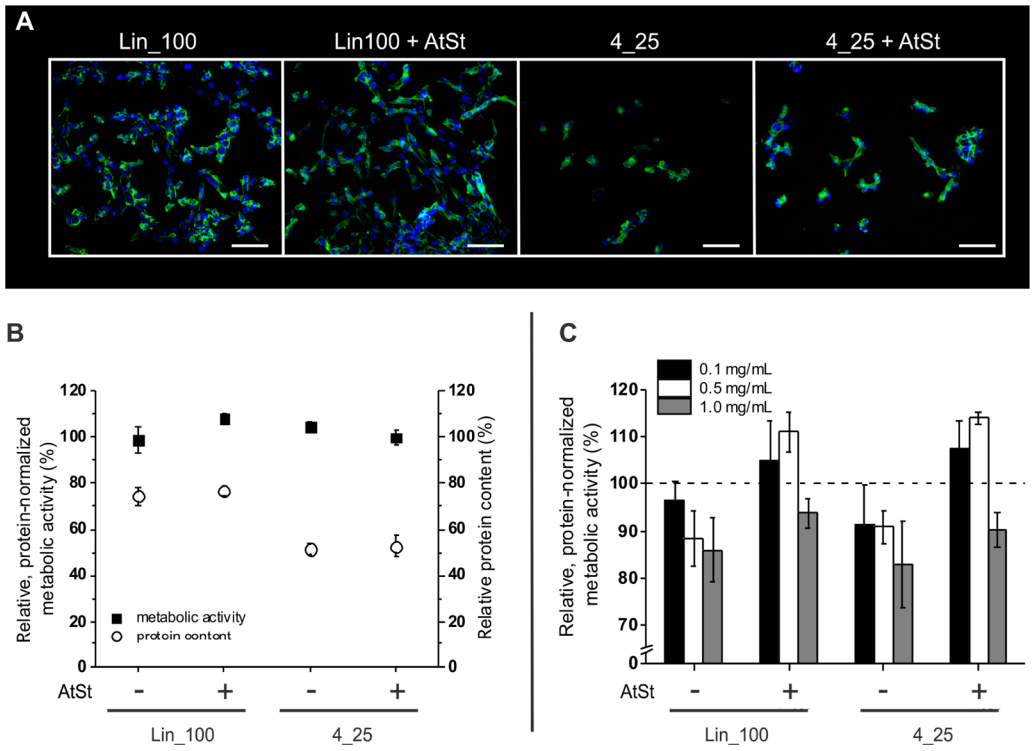

Figure 7. (A) Fluorescence microscopy images of NHOst cells grown on Lin_100 or 4_25 films with and without 0.1% wt atorvastatin (AtSt). Cells were stained for nucleus (blue) and phalloidin (green) after 7 days of incubation on the polymer films. Scale bars (white) = 50 μm. (B) Day 3 metabolic activity/cell viability (Alamar blue assay results normalized against the protein content relative to cells grown on TCPS) and protein content (BCA assay, proportional to the cell number) of NHOst cells grown on the various PDLLA films. (C) Day 3 metabolic activity/cell viability of NHOst cells after treatment with 0.1, 0.5, and 1 mg/mL PDLLA nanoparticles with/without 1% wt atorvastatin. Please note that % loading of the nanoparticles was higher than that of films to partially balance the much smaller amount of materials.

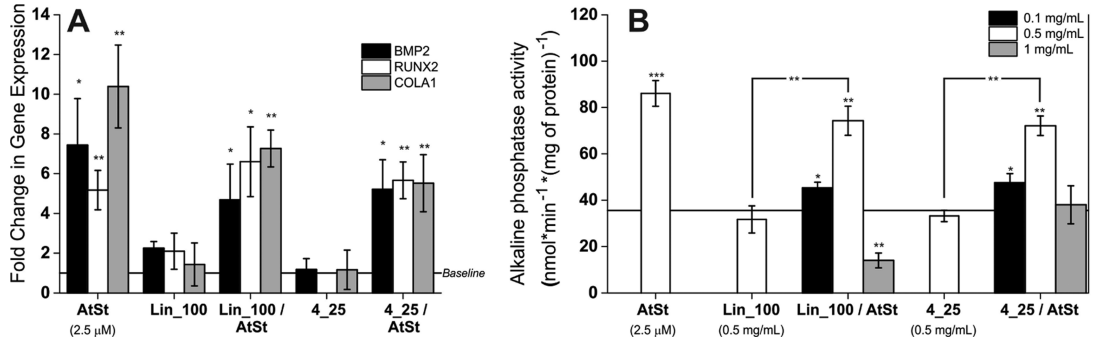

Figure 8. (A) Day 3 expression of BMP-2, RUNX2, and COLA1 genes (relative to untreated samples) determined via RT-PCR after exposure of NHOst cells to 0.5 mg/mL PDLLA nanoparticles (with/without 1% wt atorvastatin) or to free atorvastatin. (B) Alkaline phosphatase activity in NHOst cells measured after 3 days exposure to PDLLA nanoparticles and to free atorvastatin. The horizontal lines represent the baseline for both gene expression (panel A) and ALP activity (panel B).

binding and (b) any leachable material (e.g., degradation products); in experiments with nanoparticles, we predominantly assess the influence of endocyted materials.

The NHOst viability was substantially identical on Lin_100 films and on reference TCPS (polystyrene) (Figure 7B); this is not surprising since it has already been shown that the adhesion and functionality of (murine) osteoblasts on PLLA, PGA, and their blends are comparable to those on TCPS.[30] The only apparent difference is a lower cell number (75% of the control protein content); since the cells appear indistinguishable in terms of spreading, we are inclined to ascribe to a lower proliferation rate rather than to a more difficult adhesion. When the branched 4_25 was employed as a substrate, the NHOst metabolic activity was not affected, but a significant reduction in cell numbers was observed, which was also clearly visible in microscopy images (Figure 7A). This effect may be due to a lower propensity of the branched polymer to adsorb proteins from the medium, which may be ascribed to the density of hydrophilic OH groups (per gram of material), which is 4-fold higher in 4_25; however, the hydrophobic terminal dodecyl chain may also participate in higher protein adsorption on the Lin_100. Importantly, the presence of atorvastatin did not cause any significant effect either in cell metabolism or cell number.

High viability was also recorded in NHOst cells exposed for 3 days to the nanoparticles (Figure 7C), independently of the linear or branched nature of PDLLA. A decrease in viability to

DOI: 10.1021/acs.biomac.6b01524
Biomacromolecules 2017, 18, 728−739

about 85% of the control could be seen by increasing the nanoparticle concentration to 1 mg/mL; this was counteracted by the anabolic effects of atorvastatin (either released in a free form or liberated intracellularly after nanoparticle uptake) when the latter was loaded at 1% wt in both kinds of nanoparticles.

It could therefore be concluded that both the presence of a branching point and that of atorvastatin produced no significant toxic effect related to either leachable or endocyted material.

3.6. Example of Functional Behavior. The different cell adhesion on Lin_100 and 4_25 films, and the ensuing markedly different cell density did not allow a meaningful comparison of the functional behavior of these two systems; therefore the effect of atorvastatin-releasing materials on the osteoblastic activity of NHOst cells was performed only with nanoparticles.

Statins are known to upregulate critical osteogenic markers, such as bone morphogenetic protein 2 (BMP-2),[31] runtrelated gene 2 (RUNX2),[32] type I collagen (COLA1),[31] and, above all, alkaline phosphatase (ALP),[31,33] and this behavior has also been observed with simvastatin released from colloidal carriers.[34]

Here, we have first assessed the gene expression of BMP-2, RUNX2, and COLA1 in NHOst cells exposed for 3 days to nanoparticles (with/without 1% wt atorvastatin) and to atorvastatin in solution as a control (Figure 8A); the absence of any significant difference with the free drug confirmed the bioavailability and the osteogenic potential of atorvastatin loaded in nanoparticles (of both polymers).

We have then focused of the effects on ALP activity (Figure 8B). At a concentration of 0.5 mg/mL, the nonloaded particles induced no significant upregulation, whereas those loaded with atorvastatin increased it to levels comparable to those obtained with the free drug. It is noteworthy that in preliminary experiments with the free drug, we recorded little effects for concentrations below 1 μM, maximum ALP activity at a 2.5 μM, and marked reductions at concentrations of 5 μM or higher (see Supporting Information, Figure S5). A similarly narrow therapeutic window is possibly offered also by the nanoparticles: at 0.1 mg/mL the increase in ALP activity was significant but modest, at 0.5 mg/mL we observed a large increase, whereas at 1.0 mg/mL the activity dropped. In particular, with 4_25 nanoparticles the activity decreased to levels similar to the untreated samples, with for Lin_100 ones to much lower levels, mirroring the lower cell viability observed at that concentration (Figure 7C). We interpret this difference between linear and star polymers to the more rapid release of the drug from the Lin_100 nanoparticles (Figure 6A), likely leading to a higher atorvastatin concentration and therefore to a steeper drop in ALP activity at 1 mg/mL (Figure 8B). The slower release kinetics (and reduced burst release) in the branched PDLLA nanoparticles can therefore be beneficial to reduce the likelihood of drug overdosing.

4. CONCLUSION

The introduction of branching appears to significantly affect both the degradation behavior of PDLLA and the kinetics of drug release from it, both for polymer films and nanoparticles. Our results on films suggest that (a) star polymers probably degrade via a surface mechanism, with a slower kinetics than the bulk-degrading linear ones, (b) neither the functionality of the single branching point (4- or 6-armed stars) nor the degree of polymerization of the arms (25 or 50 units per arm) appeared to significantly affect these properties. It is noteworthy that the slower degradation of branched PDLLA seems to contrast with some earlier reports on other polyesters; for example, PEG-*block*-oligoesters[12] have been reported to degrade faster (see Introduction), but this may be due to the peculiarity of the PEGylated polymers, which are considerably more hydrophilic than the PDLLA studied here.

In a preliminary evaluation of these materials as potential drug releasing vehicles, the poor adhesion of cells on films of star PDLLA hampered their direct use as cell culture substrates; the nanoparticles, on the other hand, showed that linear and branched polymers allowed both for high loading efficiency and bioavailability of a model drug, i.e., atorvastatin; the slower release kinetics of the drug from 4_25 was likely responsible for the different concentration dependency of ALP activity in the linear versus branched polymer nanoparticles.

■ ASSOCIATED CONTENT

Supporting Information

The Supporting Information is available free of charge on the ACS Publications website at DOI: 10.1021/acs.biomac.6b01524.

Molecular weight distributions obtained via GPC, film thicknesses, relative elastic modulus maps acquired via AFM, a scheme of the process of nanoparticle purification, and alkaline phosphatase activity (PDF)

■ AUTHOR INFORMATION

Corresponding Authors

*E-mail: sarah.cartmell@manchester.ac.uk.
*E-mail: nicola.tirelli@manchester.ac.uk.

ORCID

Nicola Tirelli: 0000-0002-4879-3949

Notes

The authors declare no competing financial interest.

■ ACKNOWLEDGMENTS

J.B. is indebted to BBSRC for a DTP studentship, and R.D. to AstraZeneca for cofunding NoWCADD. The authors want to thank Dr. Enrique Lallana (NoWCADD) for the useful discussions and the help in NMR measurements. AFM images were acquired at the BioAFM Facility of the University of Manchester.

■ REFERENCES

(1) d'Arcy, R.; Burke, J.; Tirelli, N. Branched polyesters: Preparative strategies and applications. *Adv. Drug Delivery Rev.* **2016**, *107*, 60.

(2) Li, X. J.; Qian, Y. F.; Liu, T.; Hu, X. L.; Zhang, G. Y.; You, Y. Z.; Liu, S. Y. Amphiphilic multiarm star block copolymer-based multifunctional unimolecular micelles for cancer targeted drug delivery and MR imaging. *Biomaterials* **2011**, *32* (27), 6595−6605.

(3) Yang, X. Q.; Grailer, J. J.; Pilla, S.; Steeber, D. A.; Gong, S. Q. Tumor-Targeting, pH-Responsive, and Stable Unimolecular Micelles as Drug Nanocarriers for Targeted Cancer Therapy. *Bioconjugate Chem.* **2010**, *21* (3), 496−504.

(4) Cameron, D. J. A.; Shaver, M. P. Aliphatic polyester polymer stars: synthesis, properties and applications in biomedicine and nanotechnology. *Chem. Soc. Rev.* **2011**, *40* (3), 1761−1776.

(5) Wang, L.; Cai, C.; Dong, C.-M. Synthesis, Characterisation and Nanoparticle Formation of Star-Shaped Poly(L-Lactide) With Six Arms. *Chin. J. Polym. Sci.* **2008**, *26* (02), 161−169.

(6) Zhao, Y.; Li, J.; Yu, H.; Wang, G.; Liu, W. Synthesis and characterization of a novel polydepsipeptide contained tri-block copolymer (mPEG-PLLA-PMMD) as self-assembly micelle delivery system for paclitaxel. *Int. J. Pharm.* **2012**, *430* (1−2), 282−91.

(7) Kontoyianni, C.; Sideratou, Z.; Theodossiou, T.; Tziveleka, L. A.; Tsiourvas, D.; Paleos, C. M. A novel micellar PEGylated hyperbranched

DOI: 10.1021/acs.biomac.6b01524
Biomacromolecules 2017, 18, 728−739

polyester as a prospective drug delivery system for paclitaxel. *Macromol. Biosci.* **2008**, *8* (9), 871−81.
(8) Biela, T.; Duda, A.; Rode, K.; Pasch, H. Characterization of star-shaped poly(l-lactide)s by liquid chromatography at critical conditions. *Polymer* **2003**, *44* (6), 1851−1860.
(9) Kang, N.; Leroux, J.-C. Triblock and star-block copolymers of N-(2-hydroxypropyl)methacrylamide or N-vinyl-2-pyrrolidone and d,l-lactide: synthesis and self-assembling properties in water. *Polymer* **2004**, *45* (26), 8967−8980.
(10) Kricheldorf, H. R.; Ahrensdorf, K.; Rost, S. Polylactones, 68. *Macromol. Chem. Phys.* **2004**, *205* (12), 1602−1610.
(11) Kissel, T.; Brich, Z.; Bantle, S.; Lancranjan, I.; Nimmerfall, F.; Vit, P. Parenteral depot-systems on the basis of biodegradable polyesters. *J. Controlled Release* **1991**, *16* (1), 27−41.
(12) Breitenbach, A.; Li, Y. X.; Kissel, T. Branched biodegradable polyesters for parenteral drug delivery systems. *J. Controlled Release* **2000**, *64* (1−3), 167−78.
(13) Breitenbach, A.; Pistel, K. F.; Kissel, T. Biodegradable comb polyesters. Part II. Erosion and release properties of poly(vinyl alcohol)-g-poly(lactic-co-glycolic acid). *Polymer* **2000**, *41* (13), 4781−4792.
(14) Ghassemi, A. H.; van Steenbergen, M. J.; Barendregt, A.; Talsma, H.; Kok, R. J.; van Nostrum, C. F.; Crommelin, D. J. A.; Hennink, W. E. Controlled Release of Octreotide and Assessment of Peptide Acylation from Poly(D,L-lactide-co-hydroxymethyl glycolide) Compared to PLGA Microspheres. *Pharm. Res.* **2012**, *29* (1), 110−120.
(15) McKay, A.; Leung, B. P.; McInnes, I. B.; Thomson, N. C.; Liew, F. Y. A novel anti-inflammatory role of simvastatin in a murine model of allergic asthma. *J. Immunol.* **2004**, *172* (5), 2903−2908.
(16) Paumelle, R.; Blanquart, C.; Briand, O.; Barbier, O.; Duhem, C.; Woerly, G.; Percevault, F.; Fruchart, J. C.; Dombrowicz, D.; Glineur, C.; Staels, B. Acute antiinflammatory properties of statins involve peroxisome proliferator-activated receptor-alpha via inhibition of the protein kinase C signaling pathway. *Circ. Res.* **2006**, *98* (3), 361−369.
(17) Mundy, G.; Garrett, R.; Harris, S.; Chan, J.; Chen, D.; Rossini, G.; Boyce, B.; Zhao, M.; Gutierrez, G. Stimulation of bone formation in vitro and in rodents by statins. *Science* **1999**, *286* (5446), 1946−1949.
(18) Oryan, A.; Kamali, A.; Moshiri, A. Potential mechanisms and applications of statins on osteogenesis: Current modalities, conflicts and future directions. *J. Controlled Release* **2015**, *215*, 12−24.
(19) Jadhav, S. B.; Jain, G. K. Statins and osteoporosis: new role for old drugs. *J. Pharm. Pharmacol.* **2006**, *58* (1), 3−18.
(20) Piskin, E.; Isoglu, I. A.; Bolgen, N.; Vargel, I.; Griffiths, S.; Cavusoglu, T.; Korkusuz, P.; Guzel, E.; Cartmell, S. In vivo performance of simvastatin-loaded electrospun spiral-wound polycaprolactone scaffolds in reconstruction of cranial bone defects in the rat model. *J. Biomed. Mater. Res., Part A* **2009**, *90A* (4), 1137−1151.
(21) Stein, E. A.; Lane, M.; Laskarzewski, P. Comparison of statins in hypertriglyceridemia. *Am. J. Cardiol.* **1998**, *81* (4A), 66B−69B.
(22) Korhonen, H.; Helminen, A.; Seppälä, J. V. Synthesis of polylactides in the presence of co-initiators with different numbers of hydroxyl groups. *Polymer* **2001**, *42* (18), 7541−7549.
(23) Kim, S. H.; Han, Y.-K.; Kim, Y. H.; Hong, S. I. Multifunctional initiation of lactide polymerization by stannous octoate/pentaerythritol. *Makromol. Chem.* **1992**, *193* (7), 1623−1631.
(24) Dong, C. M.; Qiu, K. Y.; Gu, Z. W.; Feng, X. D. Synthesis of star-shapee poly(epsilon-caprolactone)-b-poly(DL-lactic acid-alt-glycolic acid) with multifunctional initiator and stannous octoate catalyst. *Macromolecules* **2001**, *34* (14), 4691−4696.
(25) Braun, B.; Dorgan, J. R.; Dec, S. F. Infrared spectroscopic determination of lactide concentration in polylactide: An improved methodology. *Macromolecules* **2006**, *39* (26), 9302−9310.
(26) Kim, S. H.; Han, Y.-K.; Ahn, K.-D.; Kim, Y. H.; Chang, T. Preparation of star-shaped polylactide with pentaerythritol and stannous octoate. *Makromol. Chem.* **1993**, *194*, 3229−3236.
(27) Kim, E. S.; Kim, B. C.; Kim, S. H. Structural Effect of Linear and Star-Shaped Poly(L-lactic acid) on Physical Properties. *J. Polym. Sci., Part B: Polym. Phys.* **2004**, *42*, 939−946.
(28) Tsuji, H.; Hayashi, T. Hydrolytic degradation of linear 2-arm and branched 4-arm poly(DL-lactide)s: Effects of branching and terminal hydroxyl groups. *Polym. Degrad. Stab.* **2014**, *102*, 59−66.
(29) Keum, C. G.; Noh, Y. W.; Baek, J. S.; Lim, J. H.; Hwang, C. J.; Na, Y. G.; Shin, S. C.; Cho, C. W. Practical preparation procedures for docetaxel-loaded nanoparticles using polylactic acid-co-glycolic acid. *Int. J. Nanomed.* **2011**, *6*, 2225−2234.
(30) Ishaug, S. L.; Yaszemski, M. J.; Bizios, R.; Mikos, A. G. Osteoblast function on synthetic biodegradable polymers. *J. Biomed. Mater. Res.* **1994**, *28* (12), 1445−53.
(31) Maeda, T.; Matsunuma, A.; Kurahashi, I.; Yanagawa, T.; Yoshida, H.; Horiuchi, N. Induction of osteoblast differentiation indices by statins in MC3T3-E1 cells. *J. Cell. Biochem.* **2004**, *92* (3), 458−471.
(32) Qiao, L. J.; Kang, K. L.; Heo, J. S. Simvastatin promotes osteogenic differentiation of mouse embryonic stem cells via canonical Wnt/beta-catenin signaling. *Mol. Cells* **2011**, *32* (5), 437−444.
(33) Song, C. L.; Guo, Z. Q.; Ma, Q. J.; Chen, Z. Q.; Liu, Z. J.; Jia, H. T.; Dang, G. T. Simvastatin induces osteoblastic differentiation and inhibits adipocytic differentiation in mouse bone marrow stromal cells. *Biochem. Biophys. Res. Commun.* **2003**, *308* (3), 458−462.
(34) Liu, X. N.; Li, X. R.; Zhou, L.; Li, S. B.; Sun, J.; Wang, Z. L.; Gao, Y.; Jiang, Y.; Lu, H. B.; Wang, Q. B.; Dai, J. W. Effects of simvastatin-loaded polymeric micelles on human osteoblast-like MG-63 cells. *Colloids Surf., B* **2013**, *102*, 420−427.

DOI: 10.1021/acs.biomac.6b01524
Biomacromolecules 2017, 18, 728−739